NANO LETTERS

pubs.acs.org/NanoLett Letter

Giant Spin Lifetime Anisotropy and Spin-Valley Locking in Silicene and Germanene from First-Principles Density-Matrix Dynamics

Junqing Xu, Hiroyuki Takenaka, Adela Habib, Ravishankar Sundararaman,* and Yuan Ping*

Cite This: *Nano Lett.* 2021, 21, 9594−9600 Read Online

ACCESS | Metrics & More | Article Recommendations | Supporting Information

ABSTRACT: Through first-principles real-time density-matrix (FPDM) dynamics simulations, we investigated spin relaxation due to electron−phonon and electron−impurity scatterings with spin−orbit coupling (SOC) in two-dimensional Dirac materials silicene and germanene at finite temperatures. We discussed the applicability of conventional descriptions of spin relaxation mechanisms by Elliott-Yafet (EY) and D'yakonov-Perel' (DP) compared to the FPDM method, which is determined by a complex interplay of intrinsic SOC, external fields, and scattering strength. For example, the electric field dependence of the spin lifetime by FPDM is close to the DP mechanism for silicene at room temperature but similar to the EY mechanism for germanene. Because of its stronger SOC strength and buckled structure in contrast to graphene, germanene has a giant spin lifetime anisotropy and spin-valley locking effect under nonzero E_z and low temperatures. More importantly, germanene has a long spin lifetime (∼100 ns at 50 K) and an ultrahigh carrier mobility, making it advantageous for spin-valleytronic applications.

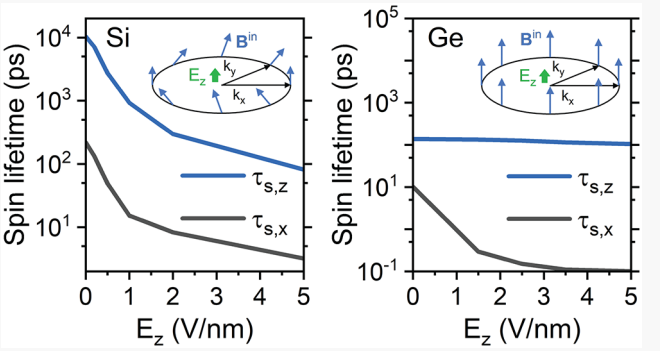

KEYWORDS: *spin lifetime, silicene, germanene, first-principles density-matrix approach, electron−phonon scattering, spin-valley locking*

INTRODUCTION

Since the discovery of graphene, significant advances have been made in the field of spintronics, exploiting spin transport instead of charge transport, with much less dissipation for low-power electronics. Several properties are key parameters for spin transport, such as long spin lifetime τ_s and diffusion length, a high carrier mobility, and the spin-valley locking (SVL) effect. Long spin lifetime and diffusion length ensure a robust spin state during propagation in a device. SVL is valuable for the emerging research field of "valleytronics",[1−3] which utilizes the valley-pseudospin as basic unit for quantum information technology.

Graphene is a very promising spintronic material,[4] with an ultrahigh mobility[5] and the longest known spin diffusion length at room temperature.[6] However, because of its weak spin−orbit coupling (SOC), SVL may be realized only through external effects, e.g., the proximity effect by interfacing with transition metal dichalcogenides (TMDs).[7,8] Other 2D materials[9] including TMDs[10] also show exciting properties for spin-/valleytronics,[1−3] for example, an ultralong spin/valley lifetime (e.g., 2 μs in p-type monolayer WSe_2 at 5 K) and a robust spin lifetime against in-plane magnetic fields, a signature of the SVL effect. However, TMDs have much lower mobilities than graphene, which is undesirable for electronic devices.[11,12]

Silicene and germanene have attracted significant attention because of their resemblance to and distinction from graphene.[13−17] They possess several remarkable properties, including tunable band structures by applying perpendicular electric fields E_z, high mobility[18,19] (Figure S10), quantum spin hall effects,[20,21] etc. Moreover, because of the buckled geometry, their SOC strength is highly enhanced and their electronic structure under finite E_z has similarity to TMDs: opposite spin signs in K and K' valleys, which are imposed by time-reversal symmetry, large SOC-induced band splittings, and highly polarized states. Therefore, silicene and germanene can combine the advantages of both graphene and TMDs but avoid some shortcomings such as limited spin lifetime (less than or equal to tens of nanoseconds) in graphene samples,[22,23] the absence of SVL in graphene, and low mobility in TMDs.[11,12]

Unfortunately, the potential for spin-based information technologies by silicene and germanene has yet to be demonstrated. Understanding spin dynamics and transport in materials is of key importance for spintronics and information technologies, and one key metric of useful spin dynamics is τ_s.

Received: August 28, 2021
Revised: November 7, 2021
Published: November 12, 2021

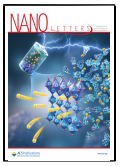

https://doi.org/10.1021/acs.nanolett.1c03345
Nano Lett. 2021, 21, 9594−9600

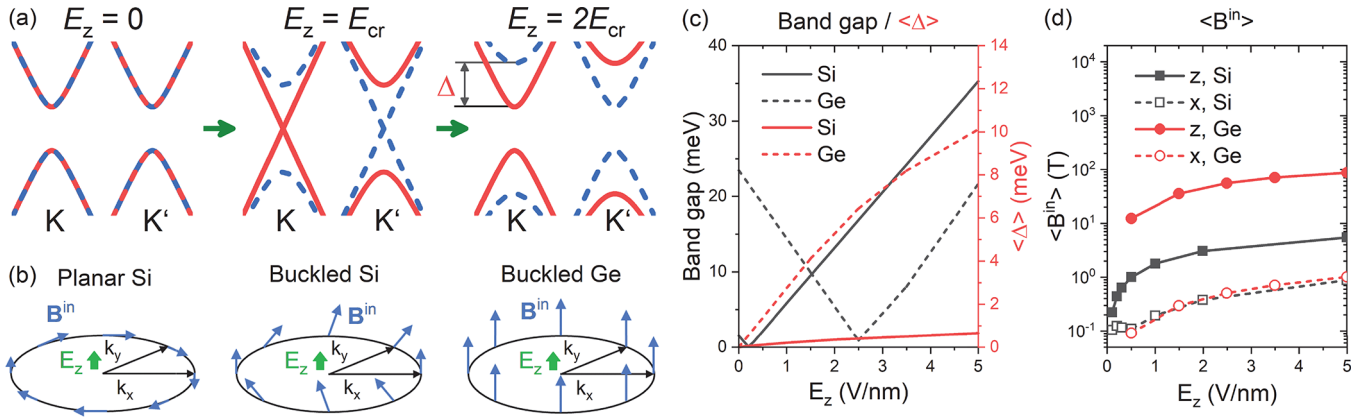

Figure 1. Electronic quantities of silicene and germanene under different perpendicular electric fields (E_z). (a) Schematic band structures under different E_z (see calculated band structures in Figures S3−S5), where E_{cr} is the critical electric field leading to zero band gap. (b) Schematic internal magnetic fields $\mathbf{B}^{in}$ (blue arrows) at a Fermi circle near one Dirac cone of planar silicene, (buckled) silicene, and (buckled) germanene induced by breaking inversion symmetry under finite E_z. $\mathbf{B}^{in}_{kn} = 2\Delta_{kn}\mathbf{S}^{exp}_{kn}/(g_e\mu_B)$, where k and n are k-point and band indices, respectively. $g_e\mu_B$ is the electron spin gyromagnetic ratio. Δ_{kn} is the energy difference between two conduction (valence) bands. $\mathbf{S}^{exp}$ is a vector and $\mathbf{S}^{exp} \equiv (S^{exp}_x, S^{exp}_y, S^{exp}_z)$, where S^{exp}_i is spin expectation value along direction i and is the diagonal element of spin matrix s_i on a Bloch basis. The spin texture of different systems under finite E_z is shown in Figure S7. (c) Band gaps (black lines) and the averaged band splitting energies $\langle\Delta\rangle$ (red lines) between two conduction/valence bands. (d) Averaged out-of-plane (B^{in}_z) and in-plane internal magnetic fields (B^{in}_x). Throughout this work, $\langle A\rangle$ means the average[24] of electronic quantity A and $\langle A\rangle = \sum_{kn} f'(\varepsilon_{kn})\, A_{kn}/\sum_{kn} f'(\varepsilon_{kn})$. f' is the derivative of the Fermi−Dirac distribution function. In this figure, for averaging, T = 300 K and the chemical potential μ is set in the middle of the band gap.

Compared with graphene, for which τ_s has been extensively studied,[6,25,26] the τ_s of silicene and germanene have not been measured and the existing few theoretical studies were done based on relatively simple models[27,28] without realistic interactions with phonons and impurities. Recently, we developed a first-principles density-matrix (FPDM) method with quantum descriptions of the scattering processes between electron−phonon (e-ph), electron−impurities (e-i), and electron−electron to simulate spin−orbit-mediated spin dynamics in solid-state systems with arbitrary symmetry.[29,30] We applied this method to disparate materials and obtained good agreement with experiments.[26,29,30] This new method enables us to predict the τ_s of silicene and germanene at finite temperatures with realistic interactions with the environment without introducing any simplified model or empirical parameters, for picosecond to microsecond time scale simulation.

RESULTS AND DISCUSSIONS

Electronic Structure. We first show electronic quantities of silicene and germanene under different E_z, which are closely related to spin dynamics and essential for understanding spin relaxation mechanisms.

Figure 1a describes schematic band structures under E_z. DFT results of band gaps and the average of band splittings $\langle\Delta\rangle$ between two conduction/valence bands are shown in Figure 1c. '$\langle\rangle$' represents taking the average of the electronic quantity (see the definition in the caption of Figure 1). At E_z = 0, because of the time-reversal and inversion symmetries, every two bands form a Kramers degenerate pair.[31] A finite E_z splits a Kramers pair because of broken inversion symmetry and band splitting increases with E_z (see Figure 1c). Moreover, as seen in Figure 1a, c, the band gap closes under a critical electric field E_{cr} (0.2 and 2.5 V/nm for silicene and germanene, respectively) and opens again above E_{cr}, corresponding to a phase transition from a topological insulator to a band insulator.[13]

The band splittings under finite E_z are effectively induced by k- and band-dependent "internal" magnetic fields $\mathbf{B}^{in}$, which are SOC fields induced by broken inversion symmetry.[31] $\mathbf{B}^{in}_{kn} \equiv 2\Delta_{kn}\mathbf{S}^{exp}_{kn}/(g_e\mu_B)$, where k and n are k-point and band indices, respectively. $g_e\mu_B$ is the electron spin gyromagnetic ratio. $\mathbf{S}^{exp} \equiv (S^{exp}_x, S^{exp}_y, S^{exp}_z)$, where S^{exp}_i is spin expectation value along direction i and is the diagonal element of the spin matrix s_i on a Bloch basis.

In Figure 1b, we depict schematics of $\mathbf{B}^{in}$ (blue arrows) near a Dirac cone of planar silicene, buckled silicene, and buckled germanene under finite E_z. In planar silicene, $\mathbf{B}^{in}$ is purely in-plane, known as Rashba spin−orbit fields $\mathbf{B}^{in}_R$. $\mathbf{B}^{in}$ in buckled silicene is analogous to an admixture of $\mathbf{B}^{in}_R$ and out-of-plane field B^{in}_z, because buckled geometry results in the presence of B^{in}_z. Different from silicene, $\mathbf{B}^{in}$ in buckled germanene is fully out-of-plane. This indicates that the stronger intrinsic SOC in germanene significantly increases B^{in}_z and thus the proportion of the in-plane component diminishes. We examine the averaged B^{in} along z, $\langle B^{in}_z\rangle$, and along x, $\langle B^{in}_x\rangle$, under E_z, as shown in Figure 1d. Whereas $\langle B^{in}_x\rangle$ for silicene and germanene increases slowly with similar values, $\langle B^{in}_z\rangle$ for germanene rises much more rapidly than that for silicene because of stronger intrinsic SOC. $\mathbf{B}^{in}$ and its anisotropy B^{in}_z/B^{in}_x are crucial for spin relaxation.

Spin Relaxation under Finite E_z. Spin lifetime and the spin relaxation mechanism can be tuned by applying electric fields.[26,32] We start our theoretical study from the electric-field dependence of τ_s, which is critical for the manipulation of spin relaxation.

As we perform FPDM calculations of τ_s, it is important to understand the connection and distinction between the FPDM method and previous theoretical models developed for specific spin relaxation mechanisms, such as Elliott-Yafet (EY) and D'yakonov-Perel' (DP) mechanisms.[31] EY represents spin relaxation due to spin-flip scattering. DP is activated when inversion symmetry is broken, which results in random spin precession between adjacent scattering events. We denote their corresponding τ_s with τ^{EY}_s and τ^{DP}_s, respectively. They are often

https://doi.org/10.1021/acs.nanolett.1c03345
Nano Lett. 2021, 21, 9594−9600

approximated by simplified relations:[31,33,34] (i) $(\tau_{s,i}^{EY})^{-1} \approx 4\langle b_i^2\rangle \langle\tau_p^{-1}\rangle$ (EY relation), where τ_p is carrier lifetime. $b_i^2 = 0.5 - S_i^{exp}$ is the degree of mixture of spin-up and spin-down states, so-called "spin mixing",[31,35] and is calculated at $E_z = 0$. (ii) $(\tau_{s,i}^{DP})^{-1} \approx \langle\tau_p^{-1}\rangle^{-1}\langle\Omega^2-\Omega_i^2\rangle$ (DP relation), where $\Omega_i = g_e\mu_B B_i^{in}$ is the Larmor precession frequency[31] with B_i^{in} defined earlier. Another estimation of $(\tau_s)^{-1}$ by considering both mechanisms is[36] $(\tau_s^{E+D})^{-1} = (\tau_s^{EY})^{-1} + (\tau_s^{DP})^{-1}$. In the following, we compare FPDM calculations and these phenomenological models with first-principles inputs of τ_p, b_i^2, and Ω_i.

We first investigate out-of-plane and in-plane spin lifetime $\tau_{s,z}$ and $\tau_{s,x}$, respectively, and their anisotropy $(\tau_{s,z}/\tau_{s,x})$ at E_z = 0 and 300 K. From Figure 2a, c, we find that (i) $\tau_{s,z}$ and $\tau_{s,x}$ of

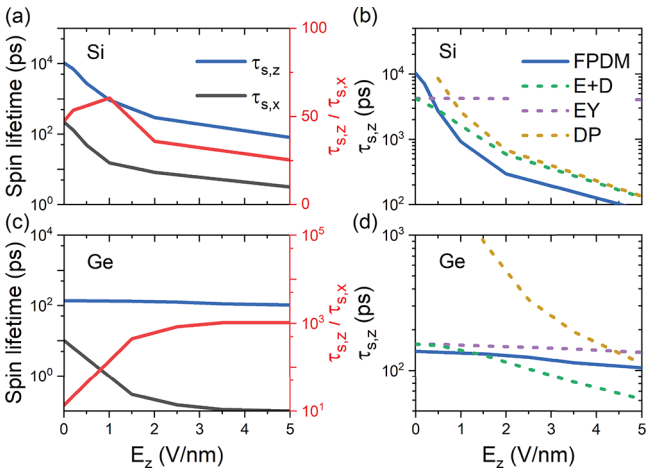

Figure 2. Spin lifetimes τ_s (left y-axis) and its anisotropy (right y-axis, red lines) of (a) intrinsic silicene and (c) intrinsic germanene as a function of E_z at 300 K. (b, d) $\tau_{s,z}$ obtained by different methods. FPDM, first-principles real-time density-matrix calculations; EY and DP correspond to $\tau_{s,z}^{EY}$ and $\tau_{s,z}^{DP}$ evaluated by EY and DP relations, respectively. E+D corresponds to $\tau_s^{E+D} = 1/[1/\tau_s^{EY} + 1/\tau_s^{DP}]$.

silicene are much longer than for germanene; (ii) large $\tau_{s,z}/\tau_{s,x}$ (10−100) is observed for both materials, much greater than the 0.5 value for graphene.[7,26] Both phenomena may be qualitatively understood based on the EY relation (typically dominant in inversion symmetric systems). Roughly speaking, the larger τ_s of silicene is mainly from the smaller b^2 compared with germanene based on their intrinsic SOC strength. Although the large $\tau_{s,z}/\tau_{s,x}$ is a result of large b_z^2/b_x^2 (Figures S6 and S8a).

We then discuss the E_z dependence of τ_s. From Figure 2a, c, the $\tau_{s,x}$ of silicene and germanene rapidly reduces with E_z. This is probably because finite E_z breaks the inversion symmetry and lifts Kramers degeneracy. This induces $\mathbf{B}^{in}$ with a rapidly increased z component as shown in Figure 1d, and thus leads to fast in-plane spin relaxation (perpendicular to B_z^{in}) and reduces $\tau_{s,x}$.

Unlike $\tau_{s,x}$, the $\tau_{s,z}$ of germanene is insensitive to E_z in Figure 2c, although the $\tau_{s,z}$ of silicene decreases quickly with E_z (Figure 2a). To better understand the E_z dependence of $\tau_{s,z}$, we compare FPDM $\tau_{s,z}$ with the model ones, $\tau_{s,z}^{EY}$, $\tau_{s,z}^{DP}$, and $\tau_{s,z}^{E+D}$, in Figure 2b, d. From Figure 2b for silicene, we show that $\tau_{s,z}^{E+D}$ and $\tau_{s,z}^{DP}$ approximately agree with FPDM $\tau_{s,z}$ in trends. For germanene, however, from Figure 2d, we find that $\tau_{s,z}^{EY}$ is in good agreement with the FPDM $\tau_{s,z}$, but neither $\tau_{s,z}^{E+D}$ nor $\tau_{s,z}^{DP}$ capture the qualitative trend. Therefore, the z-direction spin relaxation in germanene is mostly driven by the EY mechanism, and the weak E_z dependence of the $\tau_{s,z}$ of germanene may be qualitatively explained by τ_p (Figure S12) and $\tau_{s,z}^{EY}$ (Figure 2b) not being sensitive to E_z. The suppression of the DP mechanism in germanene under finite E_z may be due to the huge $\mathbf{B}^{in}$ anisotropy B_z^{in}/B_x^{in} (see Figure 1d and Figure S8b): as B_z^{in} is so strong, any in-plane spins will be quickly relaxed, and all spins are pinned along z; thus, the total spin can decay only through direct spin-flip processes but not through spin precession driven by $\mathbf{B}^{in}$, which changes the spin direction gradually.

Temperature Dependence of $\tau_{s,z}$ and Spin-Valley Locking. It is important to understand the sensitivity of τ_s to temperature and determine the optimal operating temperature.[30,38,39] Therefore, we show the temperature dependence of $\tau_{s,z}$ without E_z and with E_z = 2 and 5 V/nm (~E_{cr} + 2 V/nm) in intrinsic silicene and germanene, respectively, in Figure 3a, b. Without E_z, the $\tau_{s,z}$ of both systems increases quickly on

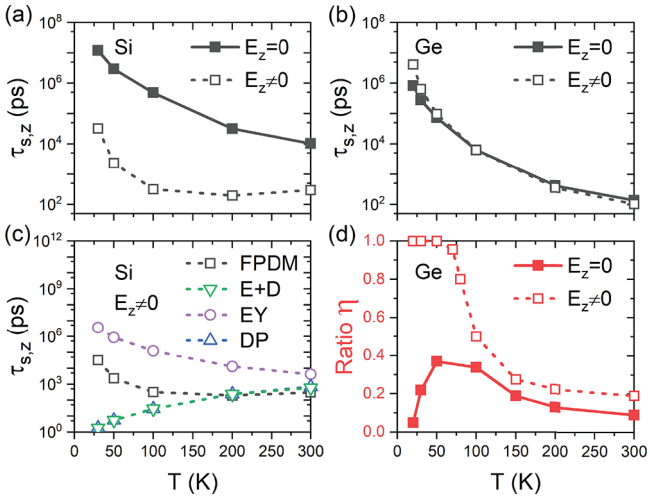

Figure 3. Temperature-dependent $\tau_{s,z}$ of intrinsic (a) silicene and (b) germanene under $E_z = 0$ and $E_z \neq 0$ (2 and 5 V/nm for silicene and germanene, respectively). (c) $\tau_{s,z}$ of intrinsic silicene under $E_z \neq 0$ obtained by different methods. The labels of the curves have the same meanings as in Figure 2. (d) Relative intervalley spin relaxation contribution η of germanene under $E_z = 0$ and $E_z \neq 0$. η is defined as $\eta = \frac{(\tau_{s,z}^{inter})^{-1}}{(\tau_{s,z}^{inter})^{-1} + w(\tau_{s,z}^{intra})^{-1}}$, where $\tau_{s,z}^{inter}$ and $\tau_{s,z}^{intra}$ are intervalley and intravalley τ_s, corresponding to scattering processes between K and K' valleys and within a single K or K' valley, respectively. η being close to 1 or 0 corresponds to intervalley or intravalley scattering dominant spin relaxation, respectively. See more details of η in ref 37.

cooling. This is the usual behavior of the EY spin lifetime simply because of the weaker e-ph scattering with lowering temperature. Because the phonon occupation is smaller at a lower temperature, τ_p is longer (Figure S12), so τ_s is longer ($\tau_s \propto \tau_p$ with the EY mechanism). Under finite E_z, the $\tau_{s,z}$ values of germanene are similar to the values under zero E_z, as shown in Figure 3b, which is expected from the discussions on the E_z dependence of germanene above. In sharp contrast, finite E_z significantly reduces the $\tau_{s,z}$ of silicene and modifies the temperature dependence. To interpret such complex temperature dependence, in Figure 3c, we compare FPDM $\tau_{s,z}$ and the model ones for silicene. All model relations fail to reproduce the temperature dependence under finite E_z for silicene. The failure of the DP relation below 200 K is probably because it is inapplicable in a weak scattering regime (weak e-ph scattering

https://doi.org/10.1021/acs.nanolett.1c03345
Nano Lett. 2021, 21, 9594−9600

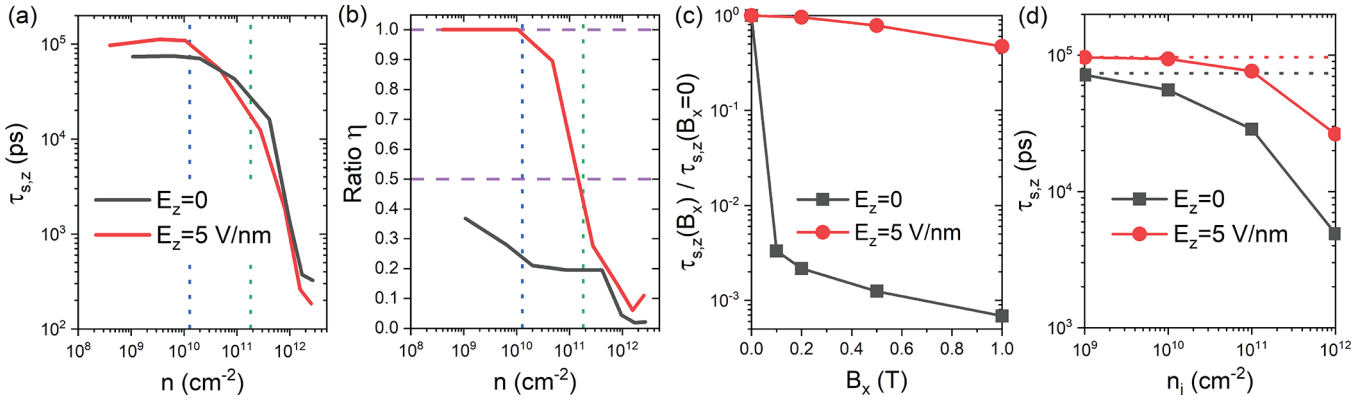

Figure 4. Spin relaxation in germanene at 50 K under 0 and 5 V/nm. (a) $\tau_{s,z}$ and (b) relative intervalley spin relaxation contribution η of germanene as a function of excess carrier density n, which is electron density n_e minus hole density n_h, and controlled by chemical potential μ. Positive carrier density corresponds to electron doping. (c) $\tau_{s,z}$ as a function of in-plane magnetic field B_x. (d) $\tau_{s,z}$ as a function of impurity density n_i of neutral Ge vacancy (with n_e and n_h kept the same as for intrinsic germanene). η being close to 1 or 0 corresponds to spin relaxation being dominated by intervalley or intravalley scattering, respectively. The blue and green dotted vertical lines correspond to μ at the minima of the first and second conduction bands, respectively. The black and red dotted lines are $\tau_{s,z}$ in the zero n_i limit under E_z = 0 and 5 V/nm, respectively.

at low temperatures ($\tau_p\langle\Omega\rangle \gtrsim 1$)).[31] Other relations have been proposed for weak scattering,[31,34,40] e.g., $\tau_s \sim |\Omega|^{-1}$, but none can capture the correct temperature dependence of the $\tau_{s,z}$ of silicene under finite E_z, e.g., $\tau_s \sim |\Omega|^{-1}$ predicts $\tau_{s,z} < 20$ ps at all temperatures investigated here. Our theoretical studies highlight the importance of simulating τ_s using the FPDM method for reliable prediction of τ_s for large variations of external conditions.

Since the bands near the Fermi energy are composed of the Dirac cones around K and K' valleys in silicene and germanene, the spin relaxation process arises from intervalley and intravalley scatterings. To scrutinize contributions of intervalley and intravalley scatterings to τ_s, we examine relative intervalley spin relaxation contribution η (see its definition in the caption of Figure 3). η being close to 1 or 0 corresponds to spin relaxation being dominated by intervalley or intravalley scattering, respectively. From Figure 3d, for germanene under E_z = 5 V/nm, η becomes close to 1 at $T \leq 70$ K. This indicates that spin relaxation is dominated by intervalley processes and is a signature of SVL. Long $\tau_{s,z}$ reaching 100 ns at 50 K and E_z = 5 V/nm indicates the stability of the spin states against spin relaxation. Contrarily, in silicene, because of the relatively small SOC splitting even at E_z = 2 V/nm as shown in Figure 1b, spin relaxation is mostly through intravalley scattering (not shown), which indicates SVL will hardly be present.

Formally, the terminology "spin-valley locking" means that the spin index (spin-up and spin-down) becomes locked with the valley index (e.g., K or K').[41] This implies that (i) two valleys exist with opposite spin polarizations. (ii) Within one valley, spins are all highly polarized along one direction, and carriers have the same sign of spin. This needs a large SOC splitting, i.e., the spin-up and -down bands being largely separated.

Point ii will cause highly suppressed intravalley spin relaxation (i.e., relaxation through scattering processes within one valley). We explain the reason using germanene as an example: Under 5 V/nm, the SOC splitting for germanene is large, 23 meV at K. To have spins with the same sign, most of carriers should be located around the band edges (which require low temperatures and low carrier densities). The intravalley spin-flip transition between an occupied state at band edges and an empty state at the second conduction/valence band will then be rather weak at low temperatures, as phonon occupation becomes negligible (Figure S9b) at the corresponding phonon energy (comparable to SOC splitting).

For intervalley e-ph processes, the corresponding phonon wavevectors are away from Γ (e.g., around K) and the minimum phonon frequency is finite (7 meV for germanene, see Figure S9b). Therefore, with SVL, spin relaxation through e-ph scattering (mostly intervalley) will be highly suppressed leading to long τ_s, because of small phonon occupations (Figure S9b) at relatively low temperatures.

SVL also allows the utilization of previously developed valleytronic technologies to design germanene-based devices.[1,3] Our calculations provide guidance on the necessary conditions to realize SVL in germanene.

Carrier Density and Magnetic Field Dependence of $\tau_{s,z}$ for Germanene at Low T. As spin-valley locking and long $\tau_{s,z}$ were observed in intrinsic germanene at 50 K, we further investigate how they are affected by carrier density, which can be tuned by electrical gate experimentally.

In Figure 4a, we plot $\tau_{s,z}$ of germanene as a function of excess carrier density n (which is electron density n_e minus hole density n_h, and controlled by chemical potential μ). We find it is very sensitive to n at the degenerate doping range ($n \gtrsim 4 \times 10^{10}$ cm^{-2}, corresponding to μ above the conduction band minimum). As the carriers contributing to spin relaxation have higher energies when n increases, the strong n dependence of $\tau_{s,z}$ should be mainly a result of the enhanced e-ph scattering strength at higher energies (Figure S13).

Moreover, from Figure 4b, the relative intervalley spin relaxation contribution $\eta > 0.9$ at $n \leq 4 \times 10^{10}$ cm^{-2} under E_z = 5 V/nm. This indicates spin relaxation being dominated by intervalley processes and the presence of SVL at the corresponding condition, consistent with our above discussions about SVL.

We then investigate SVL effects under in-plane magnetic-field B_x. From Figure 4c at 50 K for germanene, B_x has weak effects on $\tau_{s,z}$ under finite E_z. This is because the external magnetic field is too weak compared with $\mathbf{B}^{in}$ under finite E_z. This weak B_x dependence of $\tau_{s,z}$ is often used as an experimental evidence of SVL.[10] Under E_z = 0, however, strong B_x dependence is observed. This is because without the

https://doi.org/10.1021/acs.nanolett.1c03345
Nano Lett. 2021, 21, 9594−9600

presence of $\mathbf{B}^{in}$ due to Kramers degeneracy, the external B_x will mix out-of-plane and in-plane spin relaxation.[42]

Impurity Effects and Spin Diffusion Length. As an initial theoretical investigation of impurity effects, we consider only one common neutral defect in germanene, a single Ge atom vacancy.[43] From Figure 4d, we observe that $\tau_{s,z}$ values are reduced by impurities and the reduction becomes significant when impurity density n_i approaches 1×10^{12} cm^{-2}. Furthermore, $\tau_{s,z}$ under E_z = 5 V/nm reduces much less than that with E_z = 0. Our simulations suggest that if $n_i < 1 \times 10^{12}$ cm^{-2}, germanene can exhibit long $\tau_{s,z}$ over 100 ns at $T \leq 50$ K, especially under finite E_z.

We compute in-plane spin diffusion length $l_{\parallel,s_z}$ for the z-direction spin of germanene using the relation[31] $l_{\parallel,s_z} = \sqrt{D\tau_{s,z}}$, where D is the diffusion coefficient. D is estimated using the Einstein relation[44] $D = \overline{\mu}_c(n_e + n_h)/\frac{d(n_e+n_h)}{d\mu}$, where $\overline{\mu}_c$ is the average of the electron and hole mobility, which are obtained from first principles by solving the Boltzmann equation (Section SVI in the Supporting Information). From Table 1, we can see at 300 K $l_{\parallel,s_z}$ of germanene is 2−3 μm, shorter than the longest measured value of ∼12 μm for the graphene samples.[6] At 50 K, as mobilities are higher and $\tau_{s,z}$ values are longer, $l_{\parallel,s_z}$ exceeds 100 μm with $n_i \leq 1 \times 10^{11}$ cm^{-2}, much longer than experimental values of graphene, which range from 1 to 40 μm at different temperatures.[9]

Table 1. Spin Dynamic and Transport Properties of Intrinsic Germanene under E_z = 5 V/nm without and with Neutral Impurities (with Impurity Density n_i).[a]

T (K)	n_i (cm^{-2})	τ_p (ps)	$\overline{\mu}_c$ (cm^2/(V s))	D (cm^2/s)	$\tau_{s,z}$ (ns)	$l_{\parallel,s_z}$ (μm)
300	0	0.4	3.2×10^4	830	0.1	2.9
300	1×10^{11}	0.3	2.5×10^4	620	0.1	2.5
50	0	7.2	3.8×10^6	16700	97	400
50	1×10^{11}	1.6	4.5×10^5	2000	76	120
50	1×10^{12}	0.2	5.8×10^4	250	26	25

[a] $\tau_p \equiv 1/\langle\tau_p^{-1}\rangle$ is the carrier lifetime. $\overline{\mu}_c$ is the average of the electron and hole mobility. The method of calculating mobility is given in the Supporting Information. The theoretical results of the electron and hole mobility are given in Figure S10. D is the diffusion coefficient. $l_{\parallel,s_z}$ is spin diffusion length of z-direction spin. The formula computing D and $l_{\parallel,s_z}$ are given in the main text.

Additionally, we find both $\tau_{s,z}$ and τ_p decrease with increasing n_i, so $\tau_{s,z}$ has a positive correlation with τ_p. This trend agrees with the EY relation. However, τ_p changes much faster than $\tau_{s,z}$, which does not follow the EY relation, considering that b^2 is not affected by impurities. This indicates that the EY relation can not be used for quantitative evaluation.

CONCLUSIONS

Using our new FPDM method, we computed the spin lifetimes of two Dirac 2D materials, silicene and germanene, as a function of temperature, electrical doping, and neutral impurities, as well as applied electric and magnetic fields. We find silicene and germanene have qualitatively different spin relaxation mechanisms under finite E_z. By comparing FPDM τ_s and those estimated by phenomenological models with first-principles inputs, we find that germanene $\tau_{s,z}$ can be qualitatively understood by the EY relation with and without E_z. However, spin relaxation in silicene is complicated: Although at room temperature, the trend of E_z dependence of $\tau_{s,z}$ is captured by a combination of EY and DP relations, the temperature dependence of $\tau_{s,z}$ under finite E_z is explained by neither EY nor DP relations.

We demonstrated a giant spin lifetime anisotropy (two orders of magnitude higher than for graphene) and provided the condition for SVL with a long spin lifetime in germanene. Specifically, we show that at a low T of 50 K, the $\tau_{s,z}$ of germanene can reach 100 ns and $l_{\parallel,s_z}$ can exceed 100 μm (longer than graphene samples), if $n_i \leq 1 \times 10^{11}$ cm^{-2}. This is very promising because SVL has only been realized in either TMDs, which usually have much lower mobility, or graphene on substrates that have complexity of interfacial engineering. The realization of SVL in single materials with a long spin lifetime and an ultrahigh mobility opens up highly promising pathways for spin-valleytronic applications.

METHODS

The master equation of density matrix $\rho(t)$ due to e-ph and e-i scattering in interaction picture reads[29,30]

$$\frac{d\rho_{12}(t)}{dt} = \frac{1}{2}\sum_{345}\left\{\begin{array}{l}[I-\rho(t)]_{13}P_{32,45}(t)\rho_{45}(t)\\ -[I-\rho(t)]_{45}P^*_{45,13}(t)\rho_{32}(t)\end{array}\right\} + H.C. \quad (1)$$

where H.C. is the Hermitian conjugate. The subindex, e.g., "1", is the combined index of the k-point and band. $P(t)$ is the generalized scattering-rate matrix considering both e-ph and e-i scatterings, and is computed from e-ph and e-i matrix elements, electron and phonon energies.

All energies and matrix elements are calculated on coarse k and q meshes using the DFT software JDFTx,[45] and then interpolated to fine meshes in a basis of maximally localized Wannier functions.[46−48] Starting from an initial state with a net spin, we evolve $\rho(t)$ through eq 1 for a long enough simulation time, typically from nansecond to microsecond. Then, after obtaining spin observable $S_i(t)$ from $\rho(t)$ (eq S1) and fitting $S_i(t)$ to an exponential decay curve, the decay constant $\tau_{s,i}$ is obtained.

More technical details are given in Supporting Information Sections SI and SII and ref 29.

ASSOCIATED CONTENT

Supporting Information

The Supporting Information is available free of charge at https://pubs.acs.org/doi/10.1021/acs.nanolett.1c03345.

Technical and computational details, electronic structure, phonon dispersion, electron-impurity scattering, spin mixing, spin texture, internal magnetic field under an external E field, carrier mobility formalism and calculation details, carrier lifetime results, and time evolution of spin observable of silicene and germanene (PDF)

AUTHOR INFORMATION

Corresponding Authors

Yuan Ping − *Department of Chemistry and Biochemistry, University of California, Santa Cruz, California 95064, United States;* orcid.org/0000-0002-0123-3389; Email: yuanping@ucsc.edu

https://doi.org/10.1021/acs.nanolett.1c03345
Nano Lett. 2021, 21, 9594−9600

Ravishankar Sundararaman − *Department of Materials Science and Engineering, Rensselaer Polytechnic Institute, Troy, New York 12180, United States;* orcid.org/0000-0002-0625-4592; Email: sundar@rpi.edu

Authors

Junqing Xu − *Department of Chemistry and Biochemistry, University of California, Santa Cruz, California 95064, United States*

Hiroyuki Takenaka − *Department of Chemistry and Biochemistry, University of California, Santa Cruz, California 95064, United States*

Adela Habib − *Department of Physics, Applied Physics and Astronomy, Rensselaer Polytechnic Institute, Troy, New York 12180, United States; Theoretical Division, Los Alamos National Laboratory, Los Alamos, New Mexico 87544, United States*

Complete contact information is available at: https://pubs.acs.org/10.1021/acs.nanolett.1c03345

Author Contributions

J.X. and H.T. performed the ab initio calculations. J.X., H.T., and Y.P. analyzed the results. J.X., A.H., and R.S. implemented the computational codes. Y.P. designed and supervised all aspects of the study. All authors contributed to the writing of the manuscript.

Notes

The authors declare no competing financial interest.

■ ACKNOWLEDGMENTS

We thank Mani Chandra for helpful discussions. This work is supported by the Air Force Office of Scientific Research under AFOSR Award FA9550-YR-1-XYZQ and National Science Foundation under Grant DMR-1956015. A.H. acknowledges support from the American Association of University Women (AAUW) fellowship program. This research used resources of the Center for Functional Nanomaterials, which is a U.S. DOE Office of Science Facility, and the Scientific Data and Computing Center, a component of the Computational Science Initiative, at Brookhaven National Laboratory under Contract DE-SC0012704, the lux supercomputer at UC Santa Cruz, funded by NSF MRI grant AST 1828315, the National Energy Research Scientific Computing Center (NERSC), a U.S. Department of Energy Office of Science User Facility operated under Contract DE-AC02-05CH11231, the Extreme Science and Engineering Discovery Environment (XSEDE) which is supported by National Science Foundation Grant ACI-1548562,[49] and resources at the Center for Computational Innovations at Rensselaer Polytechnic Institute.

■ REFERENCES

(1) Schaibley, J. R.; Yu, H.; Clark, G.; Rivera, P.; Ross, J. S.; Seyler, K. L.; Yao, W.; Xu, X. Valleytronics in 2D materials. *Nat. Rev. Mater.* **2016**, *1*, 1−15.

(2) Zhang, L.; Gong, K.; Chen, J.; Liu, L.; Zhu, Y.; Xiao, D.; Guo, H. Generation and transport of valley-polarized current in transition-metal dichalcogenides. *Phys. Rev. B: Condens. Matter Mater. Phys.* **2014**, *90*, 195428.

(3) Tao, L.; Naeemi, A.; Tsymbal, E. Y. Valley-spin logic gates. *Phys. Rev. Appl.* **2020**, *13*, 054043.

(4) Han, W.; Kawakami, R. K.; Gmitra, M.; Fabian, J. Graphene spintronics. *Nat. Nanotechnol.* **2014**, *9*, 794−807.

(5) Das Sarma, S.; Adam, S.; Hwang, E. H.; Rossi, E. Electronic transport in two-dimensional graphene. *Rev. Mod. Phys.* **2011**, *83*, 407−470.

(6) Drogeler, M.; Franzen, C.; Volmer, F.; Pohlmann, T.; Banszerus, L.; Wolter, M.; Watanabe, K.; Taniguchi, T.; Stampfer, C.; Beschoten, B. Spin lifetimes exceeding 12 ns in graphene nonlocal spin valve devices. *Nano Lett.* **2016**, *16*, 3533−3539.

(7) Cummings, A. W.; Garcia, J. H.; Fabian, J.; Roche, S. Giant Spin Lifetime Anisotropy in Graphene Induced by Proximity Effects. *Phys. Rev. Lett.* **2017**, *119*, 206601.

(8) Gmitra, M.; Fabian, J. Proximity Effects in Bilayer Graphene on Monolayer WSe_2: Field-Effect Spin Valley Locking, Spin-Orbit Valve, and Spin Transistor. *Phys. Rev. Lett.* **2017**, *119*, 146401.

(9) Avsar, A.; Ochoa, H.; Guinea, F.; Özyilmaz, B.; van Wees, B. J.; Vera-Marun, I. J. Colloquium: Spintronics in Graphene and Other Two-Dimensional Materials. *Rev. Mod. Phys.* **2020**, *92*, 021003.

(10) Dey, P.; Yang, L.; Robert, C.; Wang, G.; Urbaszek, B.; Marie, X.; Crooker, S. A. Gate-Controlled Spin-Valley Locking of Resident Carriers in WSe2Monolayers. *Phys. Rev. Lett.* **2017**, *119*, 137401.

(11) Cheng, L.; Liu, Y. What limits the intrinsic mobility of electrons and holes in two dimensional metal dichalcogenides? *J. Am. Chem. Soc.* **2018**, *140*, 17895−17900.

(12) Ciccarino, C. J.; Christensen, T.; Sundararaman, R.; Narang, P. Dynamics and spin-valley locking effects in monolayer transition metal dichalcogenides. *Nano Lett.* **2018**, *18*, 5709−5715.

(13) Ezawa, M. Valley-polarized metals and quantum anomalous Hall effect in silicene. *Phys. Rev. Lett.* **2012**, *109*, 055502.

(14) Tsai, W.-F.; Huang, C.-Y.; Chang, T.-R.; Lin, H.; Jeng, H.-T.; Bansil, A. Gated silicene as a tunable source of nearly 100% spin-polarized electrons. *Nat. Commun.* **2013**, *4*, 1−6.

(15) Dávila, M. E.; Xian, L.; Cahangirov, S.; Rubio, A.; le Lay, G. Germanene: a novel two-dimensional germanium allotrope akin to graphene and silicene. *New J. Phys.* **2014**, *16*, 095002.

(16) Zhang, L.; Bampoulis, P.; Rudenko, A.; Yao, Q. v.; van Houselt, A.; Poelsema, B.; Katsnelson, M.; Zandvliet, H. Structural and electronic properties of germanene on MoS2. *Phys. Rev. Lett.* **2016**, *116*, 256804.

(17) Zhao, J.; Liu, H.; Yu, Z.; Quhe, R.; Zhou, S.; Wang, Y.; Liu, C. C.; Zhong, H.; Han, N.; Lu, J.; et al. Rise of silicene: A competitive 2D material. *Prog. Mater. Sci.* **2016**, *83*, 24−151.

(18) Shao, Z.-G.; Ye, X.-S.; Yang, L.; Wang, C.-L. First-principles calculation of intrinsic carrier mobility of silicene. *J. Appl. Phys.* **2013**, *114*, 093712.

(19) Ye, X.-S.; Shao, Z.-G.; Zhao, H.; Yang, L.; Wang, C.-L. Intrinsic carrier mobility of germanene is larger than graphene's: first-principle calculations. *RSC Adv.* **2014**, *4*, 21216−21220.

(20) Liu, C.-C.; Feng, W.; Yao, Y. Quantum Spin Hall Effect in Silicene and Two-Dimensional Germanium. *Phys. Rev. Lett.* **2011**, *107*, 076802.

(21) Acun, A.; Zhang, L.; Bampoulis, P.; Farmanbar, M.; van Houselt, A.; Rudenko, A. N.; Lingenfelder, M.; Brocks, G.; Poelsema, B.; Katsnelson, M. I.; Zandvliet, H. J. W. Germanene: the germanium analogue of graphene. *J. Phys.: Condens. Matter* **2015**, *27*, 443002.

(22) Han, W.; Kawakami, R. K. Spin relaxation in single-layer and bilayer graphene. *Phys. Rev. Lett.* **2011**, *107*, 047207.

(23) Kamalakar, M. V.; Groenveld, C.; Dankert, A.; Dash, S. P. Long distance spin communication in chemical vapour deposited graphene. *Nat. Commun.* **2015**, *6*, 1−8.

(24) Restrepo, O. D.; Windl, W. Full first-principles theory of spin relaxation in group-IV materials. *Phys. Rev. Lett.* **2012**, *109*, 166604.

(25) Cummings, A. W.; Roche, S. Effects of dephasing on spin lifetime in ballistic spin-orbit materials. *Phys. Rev. Lett.* **2016**, *116*, 086602.

(26) Habib, A.; Xu, J.; Ping, Y.; Sundararaman, R. Electric Field and Substrate Effects Dominate Spin-Phonon Relaxation in Graphene. *arXiv*, 2021, arXiv:2012.11550.https://arxiv.org/abs/2012.11550 (accessed 2021-10-08).

(27) Bishnoi, B.; Ghosh, B. Spin transport in silicene and germanene. *RSC Adv.* **2013**, *3*, 26153−26159.

(28) Babaee Touski, S. Spin transport in armchair silicene nanoribbon on the substrate: The role of charged impurity. *Phys. Status Solidi B* **2019**, *256*, 1900082.
(29) Xu, J.; Habib, A.; Sundararamany, R.; Ping, Y. Ab initio Ultrafast Spin Dynamics in Solids. *Phys. Rev. B* **2021**, in press.
(30) Xu, J.; Habib, A.; Kumar, S.; Wu, F.; Sundararaman, R.; Ping, Y. Spin-Phonon Relaxation from a Universal Ab Initio Density-Matrix Approach. *Nat. Commun.* **2020**, *11*, 2780.
(31) Zutic, I.; Fabian, J.; Das Sarma, S. Spintronics: Fundamentals and Applications. *Rev. Mod. Phys.* **2004**, *76*, 323.
(32) Guimarães, M. H.; Zomer, P. J.; Ingla-Aynés, J.; Brant, J. C.; Tombros, N.; van Wees, B. J. Controlling spin relaxation in hexagonal BN-encapsulated graphene with a transverse electric field. *Phys. Rev. Lett.* **2014**, *113*, 086602.
(33) Fabian, J.; Das Sarma, S. Spin relaxation of conduction electrons in polyvalent metals: Theory and a realistic calculation. *Phys. Rev. Lett.* **1998**, *81*, 5624.
(34) Leyland, W.; Harley, R.; Henini, M.; Shields, A.; Farrer, I.; Ritchie, D. Oscillatory Dyakonov-Perel spin dynamics in two-dimensional electron gases. *Phys. Rev. B: Condens. Matter Mater. Phys.* **2007**, *76*, 195305.
(35) Kurpas, M.; Faria, P. E., Jr.; Gmitra, M.; Fabian, J. Spin-orbit coupling in elemental two-dimensional materials. *Phys. Rev. B: Condens. Matter Mater. Phys.* **2019**, *100*, 125422.
(36) Bronold, F. X.; Martin, I.; Saxena, A.; Smith, D. L. Magnetic-field dependence of electron spin relaxation in n-type semiconductors. *Phys. Rev. B: Condens. Matter Mater. Phys.* **2002**, *66*, 233206.
(37) w is a weight factor related to what percent of total S_z can be relaxed out by intravalley scattering itself. w being close to 0 and 1 corresponds to intravalley scattering that can only relax a small part of and most of the excess spin, respectively. In the Supporting Information, Section SVIII and Figure S11, we give more details about w.
(38) Yang, L.; Sinitsyn, N. A.; Chen, W.; Yuan, J.; Zhang, J.; Lou, J.; Crooker, S. A. Long-Lived Nanosecond Spin Relaxation and Spin Coherence of Electrons in Monolayer MoS2 and WS2. *Nat. Phys.* **2015**, *11*, 830−834.
(39) Kikkawa, J. M.; Awschalom, D. D. Resonant Spin Amplification in n-Type GaAs. *Phys. Rev. Lett.* **1998**, *80*, 4313.
(40) Wu, M.; Jiang, J.; Weng, M. Spin dynamics in semiconductors. *Phys. Rep.* **2010**, *493*, 61−236.
(41) Xu, X.; Yao, W.; Xiao, D.; Heinz, T. F. Spin and pseudospins in layered transition metal dichalcogenides. *Nat. Phys.* **2014**, *10*, 343−350.
(42) Wang, L.; Wu, M. Electron spin relaxation due to D'yakonov-Perel'and Elliot-Yafet mechanisms in monolayer MoS 2: role of intravalley and intervalley processes. *Phys. Rev. B: Condens. Matter Mater. Phys.* **2014**, *89*, 115302.
(43) Hastuti, D. P.; Nurwantoro, P.; et al. Stability study of germanene vacancies: The first-principles calculations. *Mater. Today Commun.* **2019**, *19*, 459−463.
(44) Kubo, R. The fluctuation-dissipation theorem. *Rep. Prog. Phys.* **1966**, *29*, 255.
(45) Sundararaman, R.; Letchworth-Weaver, K.; Schwarz, K. A.; Gunceler, D.; Ozhabes, Y.; Arias, T. A. JDFTx: Software for Joint Density-Functional Theory. *SoftwareX* **2017**, *6*, 278−284.
(46) Marzari, N.; Vanderbilt, D. Maximally Localized Generalized Wannier Functions for Composite Energy Bands. *Phys. Rev. B: Condens. Matter Mater. Phys.* **1997**, *56*, 12847.
(47) Brown, A. M.; Sundararaman, R.; Narang, P.; Goddard, W. A.; Atwater, H. A. Nonradiative Plasmon Decay and Hot Carrier Dynamics: Effects of Phonons, Surfaces, and Geometry. *ACS Nano* **2016**, *10*, 957−966.
(48) Habib, A.; Florio, R.; Sundararaman, R. Hot Carrier Dynamics in Plasmonic Transition Metal Nitrides. *J. Opt.* **2018**, *20*, 064001.
(49) Towns, J.; Cockerill, T.; Dahan, M.; Foster, I.; Gaither, K.; Grimshaw, A.; Hazlewood, V.; Lathrop, S.; Lifka, D.; Peterson, G. D.; Roskies, R.; Scott, J. R.; Wilkins-Diehr, N. XSEDE: Accelerating Scientific Discovery. *Comput. Sci. Eng.* **2014**, *16*, 62−74.

https://doi.org/10.1021/acs.nanolett.1c03345
Nano Lett. 2021, 21, 9594−9600